

A Spline-Based Stress Function Approach for the Principle of Minimum Complementary Energy

Fabian Key^{a,*}, Lukas Freinberger^a

^a*Institute of Lightweight Design and Structural Biomechanics (ILSB), TU
Wien, Karlsplatz 13, Vienna, A-1040, Austria*

Abstract

In computational engineering, ensuring the integrity and safety of structures in fields such as aerospace and civil engineering relies on accurate stress prediction. However, analytical methods are limited to simple test cases, and displacement-based finite element methods (FEMs), while commonly used, require a large number of unknowns to achieve high accuracy; stress-based numerical methods have so far failed to provide a simple and effective alternative. This work aims to develop a novel numerical approach that overcomes these limitations by enabling accurate stress prediction with improved flexibility for complex geometries and boundary conditions and fewer degrees of freedom (DOFs). The proposed method is based on a spline-based stress function formulation for the principle of minimum complementary energy, which we apply to plane, linear elastostatics. The method is first validated against an analytical power series solution and then tested on two test cases challenging for current state-of-the-art numerical schemes—a bi-layer cantilever with anisotropic material behavior and a cantilever with a non-prismatic, parabolic-shaped beam geometry. Results demonstrate that our approach, unlike analytical methods, can be easily applied to general geometries and boundary conditions, and achieves stress accuracy comparable to that reported in the literature for displacement-based FEMs, while requiring significantly fewer DOFs. This novel spline-based stress function approach thus provides an efficient and flexible tool for accurate stress prediction, with promising applications in structural analysis and numerical design.

*Corresponding author

Email address: fabian.key@tuwien.ac.at (Fabian Key)

Keywords: stress analysis, stress function, spline approximation, complementary energy, linear elastostatics

1. Introduction

Accurate stress prediction is essential to computational engineering, providing the foundation for the reliable design and safety assessment of structures in aerospace, civil, and mechanical engineering applications. Many of these applications require solving boundary value problems in elasticity, where the goal is to determine the internal state of a solid, typically described by the distributions of displacements, strains, and stresses, in response to external loads and boundary conditions.

To address these problems, a variety of analytical and numerical methods have been developed in the past decades. To set the stage for our proposed method, we begin by embedding it within this broader context of commonly used solution techniques in solid mechanics. These techniques generally fall into two broad categories: (1) those based on the differential field equations of elasticity theory (see [1, Ch. 5]), and (2) those derived from variational principles (see [2]).

The first approach begins with the fundamental elasticity relations, also referred to as *field equations*: equilibrium equations, compatibility conditions, and the elastic constitutive law. Eliminating certain field variables yields different governing equations, depending on the choice of primary unknowns. For example, eliminating strains and stresses, given strain-displacement relations and the constitutive law, yields *Navier's equations*, a set of second-order partial differential equations, for the displacement field to ensure equilibrium. This system is referred to as a *displacement formulation* and provides three equations for the three unknown displacement components. It is particularly well-suited when displacement boundary conditions are prescribed over the entire boundary of the domain. Conversely, eliminating strains and displacements—again using the strain-displacement relations and the constitutive law—results in the *Beltrami-Michell equations*, which govern the stress field and ensure both compatibility and equilibrium. They provide six independent equations for the six stress components and constitute a *stress formulation*. Here, only traction boundary conditions can be imposed directly. To reduce the complexity of the stress formulation, the

concept of *stress functions* is often employed. In this concept, the stress components are related to the derivatives of the (generally tensor-valued) stress function such that the equilibrium equations are automatically satisfied. As a result, the original set of six equations can be replaced by a smaller set of equations for the stress function components. The number and form of these functions are problem-dependent; for example, in the two-dimensional case, the so-called *Airy stress function* [3] expresses the stress components in terms of a single scalar function.

Based on these differential equations, analytical methods have historically played a central role in understanding elastic behavior by offering exact closed-form solutions. However, they are generally only applicable to problems with simple geometries, homogeneous material properties, and idealized boundary conditions. Among these methods, we highlight the power series approach [4], which is particularly well-suited for regular domains and will later be used to validate our approach. This method offers a systematic way to construct a polynomial approximation of the Airy stress function by applying the biharmonic compatibility equation—which results from substituting the stress function into the Beltrami-Michell equations—together with the boundary conditions. This process reduces the original doubly infinite power series to a finite polynomial form with a specific number of coefficients to be determined for the given problem.

In contrast to formulations derived from the field equations, *variational methods* provide an alternative framework by recasting elasticity problems into problems of minimizing or finding stationary values of functionals, including those based on virtual work, energy minimization, or mixed formulations such as the de-Veubeke-Hu-Washizu principle [5, 6, 7, 8]. While a variety of variational principles exist, we focus here on two fundamental approaches particularly relevant for the numerical treatment of solids: (1) the *principle of virtual displacements*, associated with the *principle of minimum potential energy*, which forms the basis of displacement-based methods; and (2) the *principle of virtual forces*, together with the *principle of minimum complementary energy*, which underpins stress-based formulations. Other mixed formulations involving multiple independent fields—such as the *Hellinger-Reissner* principle [9, p. 654–655], [10, 11], which introduces displacements and stresses as independent variables—are especially relevant for plate and shell models, but are not discussed further here.

These principles form the basis for a variety of numerical methods that

deliver approximate solutions by applying the minimization or stationarity condition to determine the unknown coefficients in a chosen ansatz, often expressed using a finite set of basis functions. The most widely used approach is the *displacement-based finite element method (FEM)*, which is based on the principle of virtual displacements (see, e.g., [12, Ch. 2]), closely related to the principle of minimum potential energy. The FEM approximates the displacement field using piecewise polynomial basis functions over a mesh of finite elements, resulting in a sparse system of algebraic equations. Due to its robustness, flexibility, and ability to handle complex geometries and boundary conditions, FEM has become the standard computational tool in structural mechanics and many other engineering disciplines. However, stresses are obtained only indirectly by differentiation of the displacement solution. Since standard FEM employs basis functions with only C^0 inter-element continuity, the resulting stress field is generally discontinuous across element boundaries or requires post-processing with stress recovery techniques. As a result, achieving accurate stress predictions often necessitates fine meshes and, consequently, a large number of degrees of freedom (DOFs). An approach that provides higher inter-element continuity is *isogeometric analysis (IGA)* [13, 14]. It uses spline-based basis functions, such as B-Splines or non-uniform rational B-Splines (NURBS) with increased smoothness. This enhanced continuity improves the quality of the displacement field, which in turn leads to more accurate stress approximations. Still, IGA is predominantly applied as a displacement-based method in solid mechanics.

While displacement-based methods only allow to compute stresses indirectly, stress-based methods directly approximate the stress field. These methods are based on the principle of virtual forces or the principle of minimum complementary energy. To this end, *stress-based FEMs* have been developed. Early works introduced stress elements with assumed stress functions that satisfy the equilibrium conditions in their interior [15, 5, 16]. To determine the unknown coefficients, the algebraic equations were derived from the principle of minimum complementary energy, using the necessary condition of stationarity. Subsequent work extended this framework to applications with material nonlinearity, such as the incremental complementary energy approach proposed in [17], which used a stress function with 36 unknowns per rectangular element. Similarly, extensions to elastoplastic analysis were presented in [18]. For a more comprehensive review of stress-function formulations using the complementary energy principle within FEM, we refer

the reader to the overview in [19, p. 117]

Later developments in stress-based FEM focused on refining element formulations and improving the treatment of equilibrium and boundary conditions. For example, penalty formulations have been studied to incorporate inter-element constraints on stress-function elements, but choosing the right penalty factor is critical for accuracy and remains a nontrivial task [20]. Additionally, rectangular elements with 24 DOFs and triangular elements with 18 DOFs were presented, enforcing traction boundary conditions via Lagrange multipliers [21]. While effective, the use of Lagrange multipliers leads to a significant increase in the number of equations. To address the complications of prescribing traction boundary conditions, a class of element families was developed in which such conditions are satisfied directly: the so-called boundary traction elements (BTEs) and higher-order rectangular elements (HREs), with single elements ranging from 16 to 24 DOFs [22, 19]. Furthermore, an axisymmetric formulation for the analysis of circular cylindrical shells under linear deformation was presented [23]. In this approach, the three-dimensional equilibrium equations and traction boundary conditions are satisfied a priori by a tensor-valued stress function, rendering Lagrange multipliers or penalty terms unnecessary. Recent years have seen a continued interest in the development and refinement of stress-based FEMs. Building on the work in [15], a hybrid stress-function (HS-F) element method for planar problems has been developed, introducing 8- and 12-node quadrilateral elements with 16 to 24 DOFs [24]. Additionally, a strategy for modeling singular stress fields in unilateral materials that is capable of capturing stress singularities independently of the mesh resolution has been presented [25]. Further elements have been designed for different applications such as thermoelastic triangular elements [26] or beam elements with five and six DOFs per element and using Lagrange multipliers [27].

Beyond the development of new elements, a complementary energy variational approach has been presented, which approximates plane elastic problems, i.e., the behavior of a 2D continuum body, through truss structures and supports stress concentrations or singularities [28, 29]. Furthermore, a machine learning approach for linear elasticity—referred to as deep complementary energy method (DCEM)—has also been presented, in which the stress function is parameterized using three separate neural networks [30]. Nonetheless, this method entails considerable training effort, especially to accurately predict stresses and generalize to different loading scenarios.

Despite demonstrating improved accuracy in stress prediction compared to displacement-based methods, stress-based formulations based on complementary energy principles faced notable limitations. Many of the proposed elements were tailored to specific problem classes, limiting their general applicability. Additionally, the requirement to satisfy equilibrium and boundary conditions often resulted in a substantial number of equations in the final system, for example due to the high number of DOFs per element.

Lastly, we would like to mention an approach that does not fully align with the previous distinction between differential and variational methods, i.e., the application of the FEM directly to the Beltrami–Michell equations [31, 32]. Note that in this work, the equations require additional stabilization strategies to handle mixed boundary conditions effectively.

Despite the variety of methods available for stress prediction in elastic problems, key challenges remain. Analytical approaches following formulations based on the differential field equations are restricted to simple geometries and loading conditions, limiting their relevance for practical engineering applications. Following variational principles, displacement-based methods—including standard FEM and IGA—approximate the displacement field and compute stresses via post-processing. As a result, accurate stress prediction often requires fine meshes or additional recovery procedures, increasing computational effort. Alternatively, stress-based methods, which approximate the stress field directly, offer improved stress accuracy. However, they typically rely on specialized elements with many DOFs or involve complicated enforcement of equilibrium and boundary conditions. This lack of generality and efficiency has so far hindered their practicability and broader adoption.

These observations indicate there is still need for a more systematic and computationally efficient approach to direct stress approximation. Such an approach should maintain accuracy and handle general geometries and boundary conditions, both without excessive discretization effort.

This work aims to close this gap by introducing a novel variational method that directly approximates the stress field while ensuring equilibrium. Notably, the approach is broadly applicable to diverse geometries and loading conditions, as well as efficient in terms of the number of unknowns. The proposed approach is based on the principle of minimum complementary energy and employs a spline-based representation of the Airy stress function, yielding a direct stress-based methodology for solving linear and plane elasticity

problems. By using a stress function, equilibrium is satisfied by construction, as in earlier complementary energy methods. Building on these foundations, the method introduces two key enhancements:

1. The properties of B-splines enable the direct incorporation of traction boundary conditions into the ansatz and promote smooth stress fields
2. A general geometric mapping allows the spline formulation to be applied to complex geometries through transformation from a reference domain

Collectively, these features result in an accurate and efficient method for stress prediction, offering high flexibility with respect to geometry and boundary conditions.

2. Methodology: Variational Principle and Spline-Based Approximation

We begin with a presentation of the principle of minimum complementary energy, which forms the theoretical foundation of our approach. Subsequently, we introduce the novel spline-based stress function formulation, specifically expressing the Airy stress function using B-splines. By combining the complementary energy principle with the spline-based representation, we derive an algebraic system of equations for the spline control variables that define the stress function, from which the stress field is then obtained directly through differentiation.

2.1. The Principle of Minimum Complementary Energy

The starting point for our variational approach is the *principle of minimum complementary energy* [33, 34, 2], which formulates a minimization problem in terms of the *stress field* σ_{ij} . We consider the static case and an elastic body Ω with its boundary denoted by Γ , where surface traction \hat{t}_i and displacement \hat{u}_i are prescribed on the portions Γ^σ and Γ^u , respectively. Furthermore, we assume small deformations and infinitesimal strains, and that the relevant energy potentials exist. The principle requires to consider only stress fields σ_{ij} that are *statically admissible*, and we denote the set of all statically admissible stress fields by \mathbb{S} . In particular, this means that they are in *equilibrium* with a given body force density f_i in Ω and satisfy the

traction boundary conditions on Γ^σ :

$$\sigma_{ij,j} + f_i = 0 \quad \text{in } \Omega, \quad (1)$$

$$\sigma_{ij}n_j = \hat{t}_i \quad \text{on } \Gamma^\sigma. \quad (2)$$

Then, it can be shown for conservative systems that the total complementary energy Π^* takes a stationary value for the equilibrium configuration of the body:

$$\delta\Pi^* = 0. \quad (3)$$

With the additional condition

$$\delta^2\Pi^* > 0, \quad (4)$$

the principle of minimum complementary energy can be formulated as given in [35, Theorem 15b]:

The total complementary potential is a minimum with respect to variations in stress when the system is in its true state of equilibrium.

In this sense, we refer to the total complementary energy as a functional of the stresses $\Pi^*[\boldsymbol{\sigma}]$ and state the elastic problem as

$$\min_{\boldsymbol{\sigma} \in \mathbb{S}} \{\Pi^*[\boldsymbol{\sigma}]\}. \quad (5)$$

The total complementary energy Π^* can be divided into *internal* and *external* contributions U^* and W^* , respectively:

$$\Pi^*[\boldsymbol{\sigma}] = U^*[\boldsymbol{\sigma}] + W^*[\boldsymbol{\sigma}]. \quad (6)$$

For the linear elastic case, we use the generalized Hooke's law such that the internal complementary energy U^* is expressed as

$$U^* = \frac{1}{2} \int_{\Omega} S_{ijkl} \sigma_{ij} \sigma_{kl} \, d\Omega, \quad (7)$$

where S_{ijkl} denotes the *compliance tensor*. Note that Equation (4) follows if the compliance tensor \mathbf{S} is positive definite. For completeness, we also present the expressions for the external complementary energy:

$$W^* = - \int_{\Omega} u_i f_i \, d\Omega - \int_{\Gamma^u} \hat{u}_i t_i \, d\Gamma. \quad (8)$$

2.2. Spline-Based Stress Function Approach

Building on the principle of minimum complementary energy outlined above, we now present the spline-based stress function approach. Since this principle requires the stress field to be statically admissible, both the equilibrium equations and the traction boundary conditions given in Equations (1) and (2) must be satisfied. As discussed in the introduction, the use of stress functions to enforce equilibrium is well established. Here, we extend this idea by proposing a spline-based formulation of the stress function to additionally satisfy the traction boundary conditions by construction.

2.2.1. Stress Functions and the Airy Stress Function

The concept of stress functions aims to satisfy the equilibrium conditions by providing a representation of the stress field in the following form [1, Ch. 13.6]:

$$\sigma_{ij} = F_{ij} \{ \Phi \}, \quad (9)$$

with F_{ij} and Φ being a differential operator and the tensor-valued stress function, respectively. If these elements are chosen in a way that the equilibrium equations from Equation (1) are always satisfied, it is given in a *self-equilibrated* form.

For plane strain and plane stress problems, the *Airy stress function* [3] is a special scalar-valued stress function that we denote by $\varphi = \varphi(x, y)$. At this stage, no assumptions are made regarding the form of φ , which is treated as arbitrary. If we assume that the body forces can be derived from a *potential* V as

$$f_x = -\frac{\partial V}{\partial x}, \quad f_y = -\frac{\partial V}{\partial y}, \quad (10)$$

the components of the stress tensor $\boldsymbol{\sigma}$ are defined through second-order derivatives of φ :

$$\sigma_x = \frac{\partial^2 \varphi}{\partial y^2} + V, \quad \sigma_y = \frac{\partial^2 \varphi}{\partial x^2} + V, \quad \sigma_{xy} = -\frac{\partial^2 \varphi}{\partial x \partial y}. \quad (11)$$

It can be easily checked that this representation identically satisfies the equilibrium equations. What remains is to determine a specific form of φ such that the corresponding stress field σ_{ij} also satisfies the traction boundary conditions given in Equation (2), thereby completing the static admissibility. In the following, we present how the proposed spline-based ansatz can be used to meet this requirement.

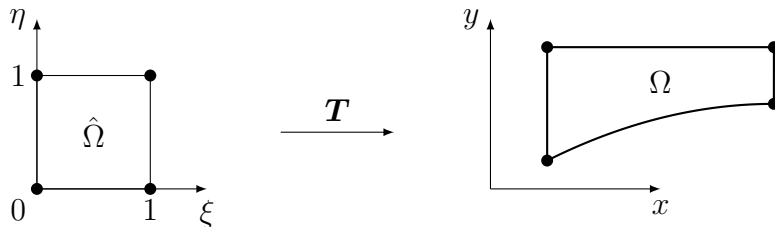


Figure 1: Geometric mapping \mathbf{T} from the parametric domain $\hat{\Omega}$ to the physical domain Ω

2.2.2. B-Spline Representation of the Airy Stress Function

To enable the spline-based representation of the Airy stress function $\varphi(x, y)$ on general, complex geometries, we begin by introducing a *geometric mapping* \mathbf{T} from a simple reference domain $\hat{\Omega}$, defined in parametric coordinates (ξ, η) , to the physical domain Ω of the elastic body, i.e., $\mathbf{T} : (\xi, \eta) \mapsto (x, y)$. An illustration of this geometric mapping is shown in Figure 1. The geometric mapping provides the foundation for expressing the stress function using B-spline basis functions defined over the parametric space. Note that this mapping is independent of the chosen ansatz for the stress function and does not have to be spline-based, although a spline-based mapping can be employed if desired.

Having established the geometric mapping between the parametric and physical domains, we define the Airy stress function $\hat{\varphi}(\xi, \eta)$ on the parametric domain such that it corresponds exactly to the physical stress function $\varphi(x, y)$ through the relation $\hat{\varphi}(\xi, \eta) = \varphi(x(\xi, \eta), y(\xi, \eta))$. This definition enables us to represent $\hat{\varphi}$ using B-spline basis functions naturally defined over the simple reference domain. The B-spline representation of $\hat{\varphi}$ is then given as follows (see [14, Equation (2.17)], for example):

$$\hat{\varphi}(\xi, \eta) = \sum_{i=1}^n \sum_{j=1}^m N_{i,p}(\xi) M_{j,q}(\eta) \hat{\phi}_{i,j}, \quad (12)$$

where $N_{i,p}(\xi)$ and $M_{j,q}(\eta)$ are univariate B-spline *basis functions* of *polynomial degrees* p and q , respectively. These basis functions form a smooth, flexible basis over the reference domain $\hat{\Omega} = [0, 1] \times [0, 1]$. The coefficients $\hat{\phi}_{i,j}$, called *control variables*, parameterize the stress function in terms of this basis. They represent the DOFs that will be determined through the

variational formulation, effectively defining the shape of the Airy stress function and thereby the stress field. The B-spline basis functions are constructed from *knot vectors*, i.e., non-decreasing sequences of coordinates ξ and η , given as $\Xi = [\xi_1, \dots, \xi_{n+p+1}]$ and $\mathcal{H} = [\eta_1, \dots, \eta_{m+q+1}]$, respectively. These knot vectors divide the reference domain in so-called *knot spans* or *elements* and, together with the control variables, represent the discretization of $\hat{\varphi}$. By combining the geometric mapping from the parametric domain to the physical domain with this spline representation, the Airy stress function can be efficiently approximated on complex geometries with a controllable level of smoothness and accuracy.

2.3. Formulation and Solution of the Elastic Problem

Based on the principle of minimum complementary energy and the spline-based representation of the Airy stress function introduced above, this section explains how to formulate and solve the resulting discrete elastic problem. First, we describe how to directly incorporate traction boundary conditions into the B-spline ansatz for the stress function, thereby ensuring the static admissibility of the solution. Then, we apply the complementary energy principle to solve for the unknown control variables, allowing us to fully define the stress function and consequently predict the stress field.

2.3.1. Traction Boundary Conditions

To incorporate the physical traction boundary conditions into the B-spline ansatz for the Airy stress function $\hat{\varphi}$, the prescribed traction must first be transformed from the physical coordinates (x, y) to the parametric coordinates (ξ, η) . Because the Airy stress function defines the physical stress components through its second-order derivatives, the traction boundary conditions directly translate into conditions on the second-order derivatives of the stress function φ in physical coordinates. To transfer them to $\hat{\varphi}$, i.e., express them in terms of the parametric coordinates, we apply the chain rule and relate the second-order derivatives in physical space to a combination of first- and second-order derivatives in the parametric space, as well as derivatives of the geometric mapping \mathbf{T} . To this end, we define \mathbf{J} as the Jacobian of the geometric mapping \mathbf{T} and its inverse \mathbf{J}^{-1} as follows:

$$\mathbf{J}(\xi, \eta) = \frac{\partial \mathbf{T}(\xi, \eta)}{\partial(\xi, \eta)} = \begin{bmatrix} \frac{\partial x}{\partial \xi} & \frac{\partial x}{\partial \eta} \\ \frac{\partial y}{\partial \xi} & \frac{\partial y}{\partial \eta} \end{bmatrix} \quad \text{and} \quad \mathbf{J}^{-1}(\xi, \eta) = \begin{bmatrix} \frac{\partial \xi}{\partial x} & \frac{\partial \xi}{\partial y} \\ \frac{\partial \eta}{\partial x} & \frac{\partial \eta}{\partial y} \end{bmatrix}. \quad (13)$$

Then, the following holds for the second-order derivatives of φ in physical space:

$$\begin{aligned} \begin{bmatrix} \frac{\partial^2 \varphi}{\partial x^2} & \frac{\partial^2 \varphi}{\partial x \partial y} \\ \frac{\partial^2 \varphi}{\partial x \partial y} & \frac{\partial^2 \varphi}{\partial y^2} \end{bmatrix} &= \mathbf{J}^{-T} \begin{bmatrix} \frac{\partial^2 \hat{\varphi}}{\partial \xi^2} & \frac{\partial^2 \hat{\varphi}}{\partial \xi \partial \eta} \\ \frac{\partial^2 \hat{\varphi}}{\partial \xi \partial \eta} & \frac{\partial^2 \hat{\varphi}}{\partial \eta^2} \end{bmatrix} \mathbf{J}^{-1} \\ &+ \begin{bmatrix} \frac{\partial^2 \xi}{\partial x^2} \frac{\partial \hat{\varphi}}{\partial \xi} + \frac{\partial^2 \eta}{\partial x^2} \frac{\partial \hat{\varphi}}{\partial \eta} & \frac{\partial^2 \xi}{\partial x \partial y} \frac{\partial \hat{\varphi}}{\partial \xi} + \frac{\partial^2 \eta}{\partial x \partial y} \frac{\partial \hat{\varphi}}{\partial \eta} \\ \frac{\partial^2 \xi}{\partial x \partial y} \frac{\partial \hat{\varphi}}{\partial \xi} + \frac{\partial^2 \eta}{\partial x \partial y} \frac{\partial \hat{\varphi}}{\partial \eta} & \frac{\partial^2 \xi}{\partial y^2} \frac{\partial \hat{\varphi}}{\partial \xi} + \frac{\partial^2 \eta}{\partial y^2} \frac{\partial \hat{\varphi}}{\partial \eta} \end{bmatrix} \end{aligned} \quad (14)$$

As a result, since the geometric mapping and all its derivatives are known and fixed by construction, the traction boundary conditions on the physical stress components—virtually given on the left-hand side of Equation (14)—translate directly into constraints on the derivatives of $\hat{\varphi}$ and, consequently, on its B-spline representation.

To build these constraints on $\hat{\varphi}$ into its B-spline ansatz, we derive conditions on the control variables $\hat{\phi}_{i,j}$. To this end, we make use of the property that the derivatives of a B-spline are also B-splines, albeit of lower degrees, and the control variables of the derivative B-splines are related to the control variables of the original B-spline through linear combinations. For example, consider the first-order derivative of $\hat{\varphi}$ with respect to the parametric coordinate ξ . Due to the differentiability properties of B-splines explained above, this derivative can be expressed as follows:

$$\frac{\partial \hat{\varphi}}{\partial \xi} = \sum_{i=1}^{n-1} \sum_{j=1}^m N_{i,p-1}(\xi) M_{j,q}(\eta) \hat{\phi}_{i,j}^{\xi}, \quad (15)$$

where $N_{i,p-1}(\xi)$ are B-spline basis functions of degree $p-1$ constructed from a modified knot Ξ^{ξ} , obtained by removing the first and last entries from the original knot vector Ξ . The control variables $\hat{\phi}_{i,j}^{\xi}$ associated with the derivative B-spline $\frac{\partial \hat{\varphi}}{\partial \xi}$ are linear combinations of the original control variables $\hat{\phi}_{i,j}$ of $\hat{\varphi}$. More specifically, the derivative control variables are given by

$$\hat{\phi}_{i,j}^{\xi} = p \frac{\hat{\phi}_{i+1,j} - \hat{\phi}_{i,j}}{\xi_{i+p+1} - \xi_{i+1}}, \quad (16)$$

where ξ_{i+p+1} and ξ_{i+1} are entries of the original knot vector Ξ . Now, suppose we want to enforce a condition on the derivative $\frac{\partial \hat{\varphi}}{\partial \xi}$ by prescribing the values

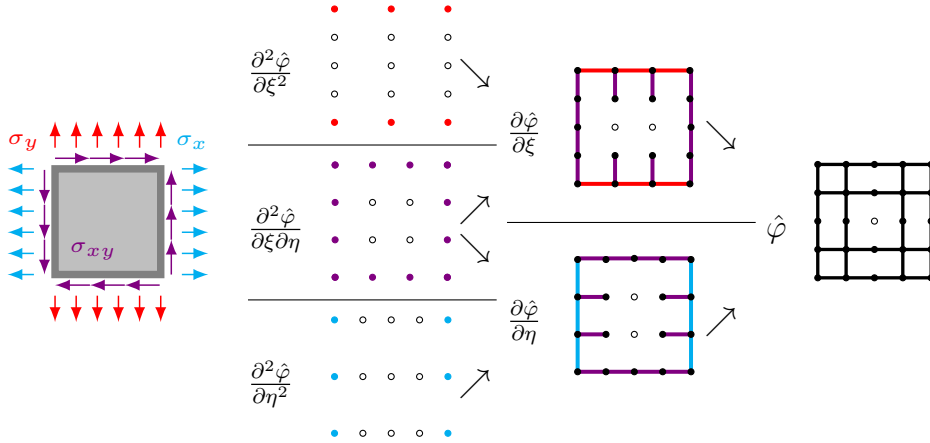


Figure 2: Incorporation of traction boundary conditions for the special case $\mathbf{T} = \text{id}$: prescribed stress components (left) and control variables for the spline-based stress function $\hat{\varphi}$ and its derivatives (right). The prescribed stress components determine the values of the marked control variables (filled circles) of the second-order derivative splines. These conditions are propagated to $\hat{\varphi}$, imposing constraints on a subset of the control variables $\hat{\phi}_{i,j}$. These constraints are indicated by lines between involved control variables. Note that, in this example, only the middle control variable of $\hat{\varphi}$ remains unconstrained.

of $\hat{\phi}_{i,j}^\xi$. Since the right-hand side of Equation (16) depends linearly on the original control variables $\hat{\phi}_{i+1,j}$ and $\hat{\phi}_{i,j}$, such a condition can be directly translated into a linear constraint on these original control variables.

This reasoning can be generalized to higher-order derivatives as well. Therefore, any condition involving first- and second-order derivatives of $\hat{\varphi}$ —such as those arising from traction boundary conditions—can be systematically propagated to a corresponding linear constraint on a subset of control variables $\hat{\phi}_{i,j}$. In particular, assembling all such conditions yields a linear system of equations that can be solved for this subset of control variables that influence the boundary behavior. After solving this system, the remaining control variables—those not involved in satisfying the traction boundary conditions—remain as the unknowns to be determined through the complementary energy principle. This process of incorporating the traction boundary conditions is illustrated in Figure 2, where, for simplicity, the special case of the identity mapping $\mathbf{T} = \text{id}$ is considered.

So, the procedure allows us to enforce certain boundary conditions in this strong sense. However, we note that, depending on the specific form of the prescribed traction, the B-spline ansatz may not be able to satisfy all

conditions exactly, but only in a weak sense. To address this, we introduce quantities that allow for the weak enforcement of a locally varying traction, a prescribed resultant force, or more general conditions. First, we define a measure $\mathfrak{D}(\hat{\phi}_{i,j})$ for the squared point-wise differences between the traction resulting from our B-spline ansatz, $t_i(\hat{\phi}_{i,j})$, and the prescribed traction, \hat{t}_i . By minimizing this measure, we enable the B-spline to approximate the boundary conditions as accurately as possible:

$$\mathfrak{D}(\hat{\phi}_{i,j}) = \int_{\Gamma^\sigma} \left| t_i(\hat{\phi}_{i,j}) - \hat{t}_i \right|^2 d\Gamma \rightarrow \min \quad (17)$$

Similarly, we define a squared residual $\mathfrak{R}(\hat{\phi}_{i,j})$ that quantifies the difference between the resultant force computed from the B-spline representation and a prescribed total force F_i , which we then aim to minimize:

$$\mathfrak{R}(\hat{\phi}_{i,j}) = \left(\int_{\Gamma^\sigma} t_i(\hat{\phi}_{i,j}) d\Gamma - F_i \right)^2 \rightarrow \min \quad (18)$$

Note that in addition to the pointwise or resultant-based traction conditions discussed above, more general constraints, such as the prescription of moments, can likewise be enforced weakly through additional terms $\mathfrak{C}(\hat{\phi}_{i,j})$. To determine the control variables that best approximate the prescribed conditions in a weak sense, we compute the minimizer of the combined error measures $\mathfrak{D}(\hat{\phi}_{i,j})$, $\mathfrak{R}(\hat{\phi}_{i,j})$, and $\mathfrak{C}(\hat{\phi}_{i,j})$. This leads to the following necessary condition for optimality:

$$\frac{\partial \left(\mathfrak{D}(\hat{\phi}_{i,j}) + \mathfrak{R}(\hat{\phi}_{i,j}) + \mathfrak{C}(\hat{\phi}_{i,j}) \right)}{\partial \hat{\phi}_{i,j}} = 0 \quad (19)$$

As before, solving the resulting equations determines the values of the control variables involved in the weak enforcement of the traction boundary conditions, while leaving the remaining ones unconstrained. We denote the set of these remaining “free” control variables by \mathbb{D} . These variables, $\hat{\phi}_{i,j} \in \mathbb{D}$, now serve as the DOFs in the subsequent minimization of the complementary energy, which we detail in the following section.

2.3.2. Minimization of the Complementary Energy

In the following, we integrate the spline-based stress function into the minimization of the complementary energy to complete the solution of the

elastic problem. After incorporating the traction boundary conditions, the remaining unknowns are the control variables $\hat{\phi}_{i,j} \in \mathbb{D}$ and we denote the stress field accordingly as $\boldsymbol{\sigma} = \boldsymbol{\sigma}(\hat{\phi}_{i,j})$. We recall that the use of a stress function, along with the enforced traction boundary conditions, guarantees static admissibility of the stress field, i.e., $\boldsymbol{\sigma}(\hat{\phi}_{i,j}) \in \mathbb{S}$. It is also important to note that displacement boundary conditions enter the formulation through the external contribution W^* to the total complementary energy (see Equation (8)). Consequently, we can reformulate the elastic problem by transforming Equation (5) into an unconstrained minimization of the total complementary energy with respect to the remaining control variables $\hat{\phi}_{i,j} \in \mathbb{D}$:

$$\min_{\hat{\phi}_{i,j} \in \mathbb{D}} \left\{ \Pi^* \left[\boldsymbol{\sigma} \left(\hat{\phi}_{i,j} \right) \right] \right\}. \quad (20)$$

Rather than solving the minimization problem in Equation (20) directly, we can instead employ the necessary condition for optimality:

$$\frac{\partial \Pi^*}{\partial \hat{\phi}_{i,j}} = 0, \quad (21)$$

which yields a system of linear equations for the unknown control variables $\hat{\phi}_{i,j} \in \mathbb{D}$. We note that if the traction boundary conditions are enforced weakly, the necessary conditions for optimality from Equations (19) and (21) (boundary conditions and complementary energy) can also be combined into a single system.

Since we consider only plane problems, we adopt the following matrix-vector notation for the stress-strain relationship, relating the vectors of stress and strain components given by $(\sigma_{xx}, \sigma_{yy}, \sigma_{xy})^T$ and $(\varepsilon_{xx}, \varepsilon_{yy}, \varepsilon_{xy})^T$, respectively:

$$(\varepsilon_{xx}, \varepsilon_{yy}, \varepsilon_{xy})^T = \mathcal{S} (\sigma_{xx}, \sigma_{yy}, \sigma_{xy})^T, \quad (22)$$

where \mathcal{S} is the compliance tensor in matrix form. For instance, in the case of plane stress, the compliance matrix takes the form

$$\mathcal{S} = \frac{1}{E} \begin{pmatrix} 1 & -\nu & 0 \\ -\nu & 1 & 0 \\ 0 & 0 & 1 + \nu \end{pmatrix}, \quad (23)$$

where E and ν denote Young's modulus and Poisson's ratio, respectively.

In summary, the proposed method to solve the elastic problem proceeds by combining the spline-based representation of the stress function with the variational formulation based on complementary energy. The overall approach can be outlined as follows:

1. **Define the geometric mapping:** For a given problem geometry, construct a geometric mapping \mathbf{T} that transforms the reference domain $\hat{\Omega}$ into the physical domain Ω of the elastic body.
2. **Specify the B-spline stress function:** Define the B-spline representation of the stress function $\hat{\varphi}$ in the parametric domain, choosing the polynomial degrees p and q , the number of control variables n and m , and the associated knot vectors Ξ and \mathcal{H} .
3. **Incorporate traction boundary conditions:** Enforce the traction boundary conditions either strongly (by directly imposing constraints) or weakly (e.g., by minimizing residuals), resulting in a system of equations for the control variables $\hat{\phi}_{i,j}$. Solving this system determines the constrained control variables and identifies the remaining unconstrained ones, denoted as $\hat{\phi}_{i,j} \in \mathbb{D}$.
4. **Minimize the total complementary energy:** Using the previously defined B-spline ansatz for the stress function, the total complementary energy Π^* from Equation (6) becomes a scalar expression depending only on the unconstrained control variables $\hat{\phi}_{i,j} \in \mathbb{D}$. To determine these unknowns, minimize the total complementary energy directly as formulated in Equation (20), or solve the associated optimality condition in Equation (21). This final step fully determines the stress function $\hat{\varphi}$.
5. **Compute the physical stress field:** Finally, the components of the stress tensor $\boldsymbol{\sigma}$ are obtained as second-order derivatives of the Airy stress function φ , by evaluating the derivatives of $\hat{\varphi}$ in the parametric domain and applying the chain rule using the derivatives of the geometric mapping.

Before applying this approach to practical test cases, we briefly highlight its key advantages. First, the spline-based ansatz for the stress function offers flexibility in choosing polynomial degrees, ensuring high-order continuity of the stress function and, thus, a smooth stress distribution throughout the domain. This eliminates the need for additional inter-element treatment commonly required in the existing methods, allowing for relatively low

number of unknowns. Furthermore, traction boundary conditions can be seamlessly integrated into the B-spline stress function formulation by leveraging the relationship between the control variables of a B-spline and its derivatives. Finally, the geometric mapping allows for the representation of complex-shaped domains while preserving the formulation in the parametric space, combining flexibility with conceptual simplicity. Together, these features position the spline-based approach as a flexible and efficient alternative for solving elasticity problems using a stress function within the principle of minimum complementary energy framework.

3. Results and Discussion

To illustrate the functionality of the proposed approach, we begin by validating our method against an analytical solution obtained via the power series approach. This comparison focuses on the stress distributions to demonstrate the accuracy of the spline-based formulation. Subsequently, we consider two test cases in which accurate stress prediction remains challenging for existing numerical methods: (1) a bi-layer cantilever with anisotropic material behavior and (2) a parabolic-shaped cantilever as an example for non-prismatic beams, illustrating the application of the approach to problems with non-regular geometries. In these examples, we evaluate both the accuracy of the resulting stress fields and the efficiency of the method by comparing the final number of unknowns required in our formulation.

3.1. Bending of a Beam by Uniform Transverse Loading

As a first test case, we consider the classical problem of a rectangular beam subjected to uniform transverse loading under plane stress conditions. This example is taken from a textbook [1, Example 8.3], which provides a polynomial solution following the power series approach. We take this as a reference solution to validate our approach by comparing the resulting stress fields. The test case models the bending of a beam subjected to a uniform transverse load w applied along its top surface. The beam has a rectangular shape with total length $2l$ and total height $2c$, where l and c denote the half-length and half-height, respectively. Additionally, we assume a unit out-of-plane depth. The values for the dimensions and the loading are given in Table 1. The boundary conditions are given as follows. Pointwise boundary conditions are applied on the top and bottom surfaces, while the ends of the beam are treated with simplified, statically equivalent boundary conditions.

l (m)	c (m)	l/c (-)	w (N m ⁻¹)	E (Pa)	ν (-)
3	0.25	12	1	1×10^5	0.3

Table 1: Bending of a beam by uniform transverse loading: dimensions, loading, and material parameters.

	Horizontal	Vertical	Moment
Top	$\sigma_{xy} = 0$	$\sigma_y = -w$	-
Bottom	$\sigma_{xy} = 0$	$\int_{-l}^l \sigma_y = 0$	-
Left	$\int_{-c}^c \sigma_x dy = 0$	$\int_{-c}^c \sigma_{xy} dy = +wl$	$\int_{-c}^c \sigma_{xy} dy = 0$
Right	$\int_{-c}^c \sigma_x dy = 0$	$\int_{-c}^c \sigma_{xy} dy = -wl$	$\int_{-c}^c \sigma_{xy} dy = 0$

Table 2: Bending of a beam by uniform transverse loading: boundary conditions.

This is due to the fact that the polynomial ansatz cannot satisfy general boundary conditions exactly. To address this issue, the complex, often explicitly unknown, boundary conditions are replaced by statically equivalent polynomial conditions in accordance with the Saint-Venant principle. As a result, the solution is expected to be accurate primarily in regions sufficiently far from the boundaries where these simplifications are applied. In this case, the simplified boundary conditions at the ends of the beam include zero resultant horizontal forces and bending moments, and a vertical resultant force ensuring global equilibrium. The complete set of boundary conditions is summarized in Table 2 and the geometry is illustrated in Figure 3.

The polynomial ansatz for the Airy stress function used in the reference solution is:

$$\varphi^{\text{ref}}(x, y) = A_{20}x^2 + A_{21}x^2y + A_{03}y^3 + A_{23}x^2y^3 - \frac{A_{23}}{5}y^5, \quad (24)$$

where A_{20} , A_{21} , A_{03} , and A_{23} are constant coefficients. These coefficients can be determined using the boundary conditions and the biharmonic equation

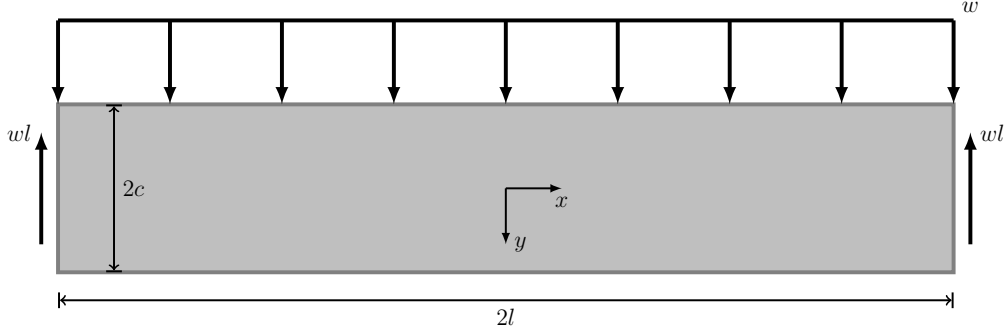


Figure 3: Bending of a beam by uniform transverse loading: setup.

such that the stress components are given as:

$$\sigma_{xx}^{\text{ref}} = \frac{3w}{4c} \left(\frac{l^2}{c^2} - \frac{2}{5} \right) y - \frac{3w}{4c^3} \left(x^2 y - \frac{2}{3} y^3 \right), \quad (25)$$

$$\sigma_{yy}^{\text{ref}} = -\frac{w}{2} + \frac{3w}{4c} y - \frac{w}{4c^3} y^3, \quad (26)$$

$$\sigma_{xy}^{\text{ref}} = -\frac{3w}{4c} x + \frac{3w}{4c^3} x y^2. \quad (27)$$

To derive the spline-based solution, we begin with defining the geometric mapping \mathbf{T} as follows:

$$\begin{pmatrix} x \\ y \end{pmatrix} = \mathbf{T}(\xi, \eta) = \begin{pmatrix} (2\xi - 1)l \\ (1 - 2\eta)c \end{pmatrix}. \quad (28)$$

Next, we specify the ansatz for the stress function $\hat{\varphi}$. For the B-spline basis functions, we choose the polynomial degrees $p = 2$ and $q = 5$ to match the highest exponents in x and y appearing in the reference Airy stress function φ^{ref} from Equation (24). The grid of control variables $\hat{\varphi}_{i,j}$, the so-called control net, is defined using $n = 3$ and $m = 6$ control variables, which represents the minimum number required to support the chosen degrees. Furthermore, we use uniform and open knot vectors in both dimensions. The control net is illustrated in Figure 4a. Note that the total number of unknowns in our ansatz, i.e., the number of control variables, is only $\mathcal{N} = n \cdot m = 18$.

In general, the polynomial degrees and the number of control variables can be selected based on the expected structure of the solution in a given

	Horizontal	Vertical	Moment
Top	$\int_{-l}^l \sigma_{xy}^2 dx$	$\int_{-l}^l (\sigma_y - w)^2 dx$	–
Bottom	$\int_{-l}^l \sigma_{xy}^2 dx$	$\int_{-l}^l \sigma_y^2 dx$	–
Left	$\int_{-c}^c \sigma_x^2 dy$	$\left(\int_{-c}^c \sigma_{xy} dy - wl\right)^2$	$\left(\int_{-c}^c \sigma_{xy} dy\right)^2$
Right	$\int_{-c}^c \sigma_x^2 dy$	$\left(\int_{-c}^c \sigma_{xy} dy + wl\right)^2$	$\left(\int_{-c}^c \sigma_{xy} dy\right)^2$

Table 3: Bending of a beam by uniform transverse loading: quantities to be minimized for a weak enforcement of the boundary conditions.

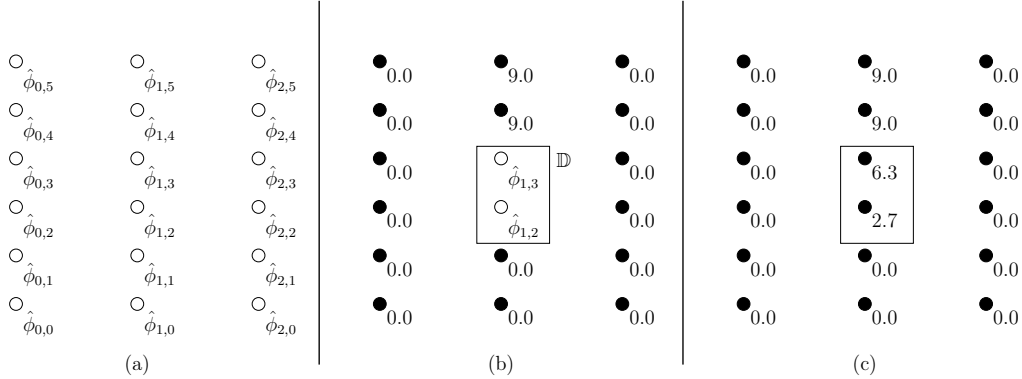


Figure 4: Bending of a beam by uniform transverse loading: control net for $\hat{\varphi}$ (a) initially, (b) after integration of the boundary conditions, and (c) after minimization of the complementary energy.

problem or determined empirically to achieve a desired level of accuracy, while keeping them as low as possible to maintain computational efficiency.

For the weak enforcement of the boundary conditions, we minimize the quantities provided in Table 3. After integration of the boundary conditions, only two control variables remain unconstrained, i.e., $|\mathbb{D}| = 2$ (see Figure 4b), and are the DOFs for the minimization of the complementary energy. In this case, we use the optimality condition and solve a linear system of equations for the remaining control variables $\hat{\varphi}_{i,j} \in \mathbb{D}$. The resulting values for the control variables are shown in Figure 4c.

Finally, we can evaluate the second-order derivatives of φ to obtain the stress components in the physical space. The resulting distributions of the

l/c	σ_{xx}	σ_{yy}	σ_{xy}
12	1.19×10^{-3}	4.91×10^{-5}	1.80×10^{-4}
24	2.99×10^{-4}	1.20×10^{-5}	4.43×10^{-5}
48	7.47×10^{-5}	3.00×10^{-6}	1.11×10^{-5}

Table 4: Bending of a beam by uniform transverse loading: relative differences $\varepsilon_{L^2}[\sigma_\bullet]$ between the spline-based and reference solutions for various aspect ratios l/c .

individual stress components are shown in Figure 5. As can be seen in these plots, the spline-based approach yields a smooth and continuous stress distribution throughout the entire domain, despite the relatively small number of unknowns. This demonstrates the effectiveness of the high-order continuity inherent in the spline representation, in contrast to the inter-element discontinuities that typically arise in standard FEMs.

To validate our results, we compare them with the reference solution obtained from the power series approach presented in [1, Example 8.3]. Specifically, we examine the distribution of the individual stress components across the beam’s height at two locations: the mid-span ($x = 0$ m) and closer to the right end ($x = 1.5$ m), as shown in Figure 6. Across all components, the spline-based solution exhibits excellent agreement with the reference, confirming the accuracy of the proposed method.

For a quantitative comparison, we consider the relative difference between the spline-based solution and the reference solution in the L_2 norm over the entire domain, given as

$$\varepsilon_{L^2}[\sigma_\bullet] = \left(\frac{\int_{\Omega} |\sigma_\bullet - \sigma_\bullet^{\text{ref}}|^2 \, d\Omega}{\int_{\Omega} |\sigma_\bullet^{\text{ref}}|^2 \, d\Omega} \right)^{\frac{1}{2}}, \quad (29)$$

where $\sigma_\bullet^{\text{ref}}$ denotes the stress components obtained from the power series approach $\hat{\varphi}^{\text{ref}}$ used as the reference. The resulting relative differences for the components σ_{xx} , σ_{yy} , and σ_{xy} are listed in Table 4, and amount to 1.19×10^{-3} , 2.99×10^{-4} , and 1.80×10^{-4} , respectively. These small values confirm that the spline-based approach provides highly accurate stress predictions, even with a compact representation involving only a small number of control variables. The observed differences between the spline-based solution and the polynomial reference solution can be primarily attributed to boundary effects. In our approach, boundary conditions are enforced entirely in a weak

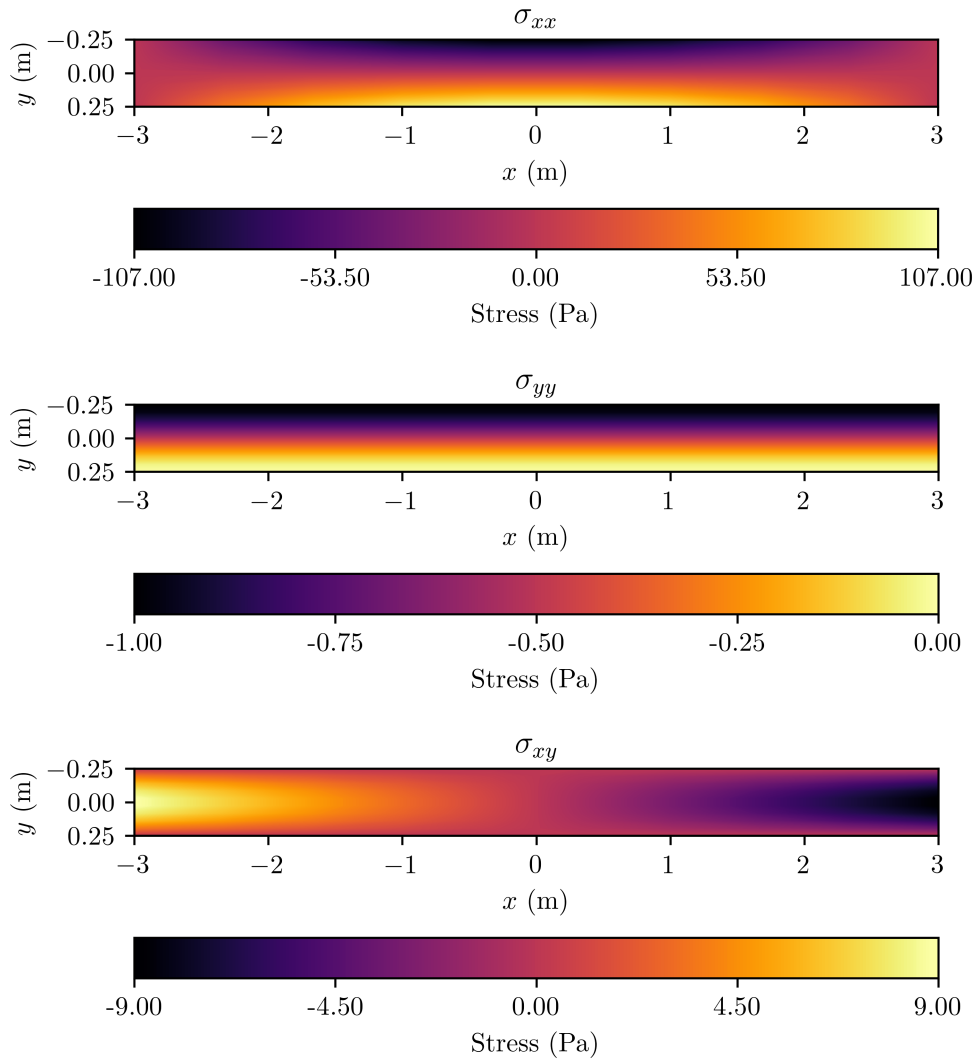


Figure 5: Bending of a beam by uniform transverse loading: stress distributions for the three stress components.

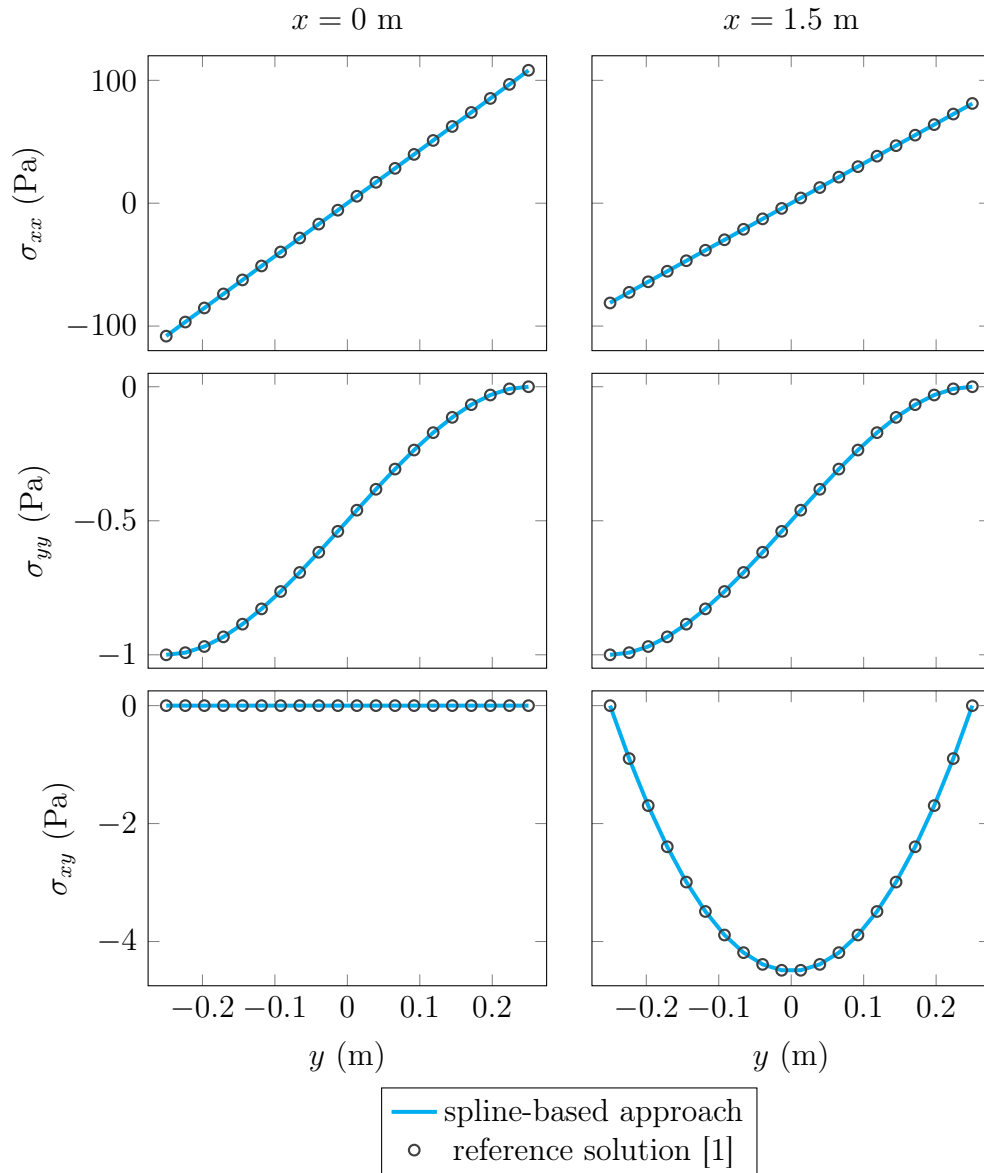


Figure 6: Bending of a beam by uniform transverse loading: comparison of the stress components across the beam's height at the mid-span (left column, $x = 0 \text{ m}$) and further along the beam (right column, $x = 1.5 \text{ m}$).

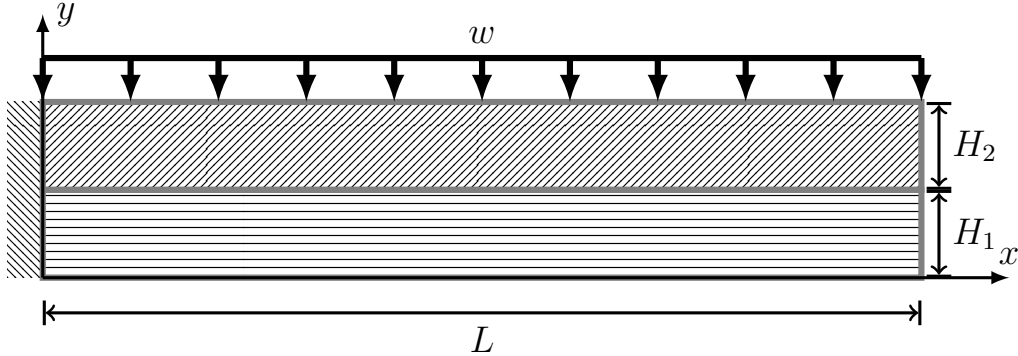


Figure 7: Bi-layer cantilever: setup.

form, whereas the reference solution uses a limited, carefully chosen set of polynomial terms designed to satisfy the simplified boundary conditions more directly—“a choice that has come from previous trial and error” [1, Example 8.3]. In contrast, the spline-based ansatz inherently includes a much broader range of polynomial terms, offering greater flexibility but potentially requiring additional constraints to better reproduce the boundary behavior seen in the reference solution. It is important to note, however, that the reference itself uses a simplification of the true boundary conditions. Therefore, attempting to exactly match the reference solution’s behavior at the boundaries is not meaningful. More importantly, the expected decrease in boundary effects with increasing beam aspect ratio l/c , as predicted by the Saint-Venant principle, should be verified, and is indeed confirmed by the data presented in Table 4.

3.2. Bi-Layer Cantilever with Anisotropic Material Behavior

After validating our method, we now turn to more challenging scenarios where accurate stress prediction is particularly demanding. In this section, we consider a multilayer planar beam with anisotropic material behavior under the plane stress assumption, as introduced in [36]. This test case is especially relevant for modeling timber and composite structures, where layered configurations and directional material properties play a critical role. Specifically, we investigate the stress prediction for a bi-layer anisotropic cantilever and perform a comparison with FEM results reported in the literature (see [36, Section 5.1]).

The setup of the problem is illustrated in Figure 7. The beam, which

L (mm)	H_1 (mm)	H_2 (mm)	w (N mm ⁻¹)	E_{11} (Pa)	E_{22} (Pa)	G_{12} (Pa)	ν (-)
500	50	50	1	10×10^9	0.5×10^9	1×10^9	0

Table 5: Bi-layer cantilever: test case settings.

has a length L and a unit depth, consists of two layers with thicknesses H_1 and H_2 , respectively, and is subjected to a uniformly distributed loading w . Each layer exhibits piecewise constant material properties and the anisotropy is described through a position-dependent compliance tensor in matrix form:

$$\mathcal{S}(y) = \mathcal{R}^T(y) \begin{bmatrix} \frac{1}{E_{11}(y)} & -\frac{\nu(y)}{E_{11}(y)} & 0 \\ -\frac{\nu(y)}{E_{11}(y)} & \frac{1}{E_{22}(y)} & 0 \\ 0 & 0 & \frac{1}{G_{12}(y)} \end{bmatrix} \mathcal{R}(y), \quad (30)$$

where $E_{11}(y)$, $E_{22}(y)$, $G_{12}(y)$, and $\nu(y)$ define the material properties in the local principal directions. The rotation matrix

$$\mathcal{R}(y) = \begin{bmatrix} \cos^2(\theta(y)) & \sin^2(\theta(y)) & \sin(2\theta(y)) \\ \sin^2(\theta(y)) & \cos^2(\theta(y)) & -\sin(2\theta(y)) \\ -\frac{\sin(2\theta(y))}{2} & \frac{\sin(2\theta(y))}{2} & \cos(2\theta(y)) \end{bmatrix}, \quad (31)$$

accounts for the rotation of the local principal axes by an angle $\theta(y)$ relative to the global x -axis. In this example, the material principal direction is aligned with the beam axis in the bottom layer ($\theta = 0^\circ$), while in the top layer it is rotated by $\theta = 15^\circ$. The values for all relevant dimensions and material parameters are summarized in Table 5.

Next, we proceed with the spline-based approach. We reflect the division of the beam into two layers by introducing separate stress functions for each region, allowing us to capture the distinct material behavior in the multilayer configuration. Specifically, we define individual stress functions, $\hat{\varphi}^{\text{bottom}}$ and $\hat{\varphi}^{\text{top}}$, along with their respective geometric mappings:

$$\mathbf{T}^{\text{bottom}}(\xi, \eta) = \begin{pmatrix} \xi L \\ \eta H_1 \end{pmatrix}, \quad \mathbf{T}^{\text{top}}(\xi, \eta) = \begin{pmatrix} \xi L \\ H_1 + \eta H_2 \end{pmatrix}. \quad (32)$$

We employ the same B-spline ansatz for both layers, using degrees $p = 2$ and $q = 4$, and control net dimensions $n = 12$ and $m = 7$, which results in a total

		Horizontal	Vertical
Top Layer	Top	$\int_0^L t_x ^2 dx$	$\int_0^L t_y + w ^2 dx$
	Right	$\int_{H_1}^{H_2} t_i ^2 dy$	
Coupling		$\int_0^L t_i^{\text{bottom}} + t_i^{\text{top}} ^2 dx$	
Bottom Layer	Bottom	$\int_0^L t_i ^2 dx$	
	Right	$\int_0^{H_1} t_i ^2 dy$	

Table 6: Bi-layer cantilever: quantities to be minimized for a weak enforcement of the boundary and coupling conditions.

of $\mathcal{N} = 2 \cdot n \cdot m = 168$ control variables. Traction boundary conditions are imposed along the top edge to realize the external loading, and zero-traction conditions are enforced on the right edge and the bottom surface. No traction is specified on the left edge, as the zero-displacement boundary condition for the clamp automatically enters the formulation through the total complementary energy, which will be minimized. To couple the two layers along the horizontal interface at $y = H_1$, we impose a coupling condition requiring the traction on either side of the internal boundary to be equal in magnitude but opposite in direction. All applied weak boundary and coupling conditions are summarized in Table 6.

The resulting stress distributions for all three components are shown in Figure 8. Due to the anisotropic material behavior, the problem gives rise to non-trivial stress distributions, even within the geometrically simple rectangular domain. As seen in the figures, the stress fields are still smooth within each individual layer. Furthermore, the components relevant for the interface coupling, σ_{yy} and σ_{xy} , are continuous across the interface, confirming the correct enforcement of the coupling. In contrast, the normal stress component σ_{xx} exhibits a clear jump at the interface, which is consistent with the discontinuous material behavior between the two layers.

To further assess the accuracy of our method, we compare the results to a reference FEM solution presented in [36, Section 5.1], which was computed using Abaqus with 4-node plane stress, fully integrated, bilinear elements

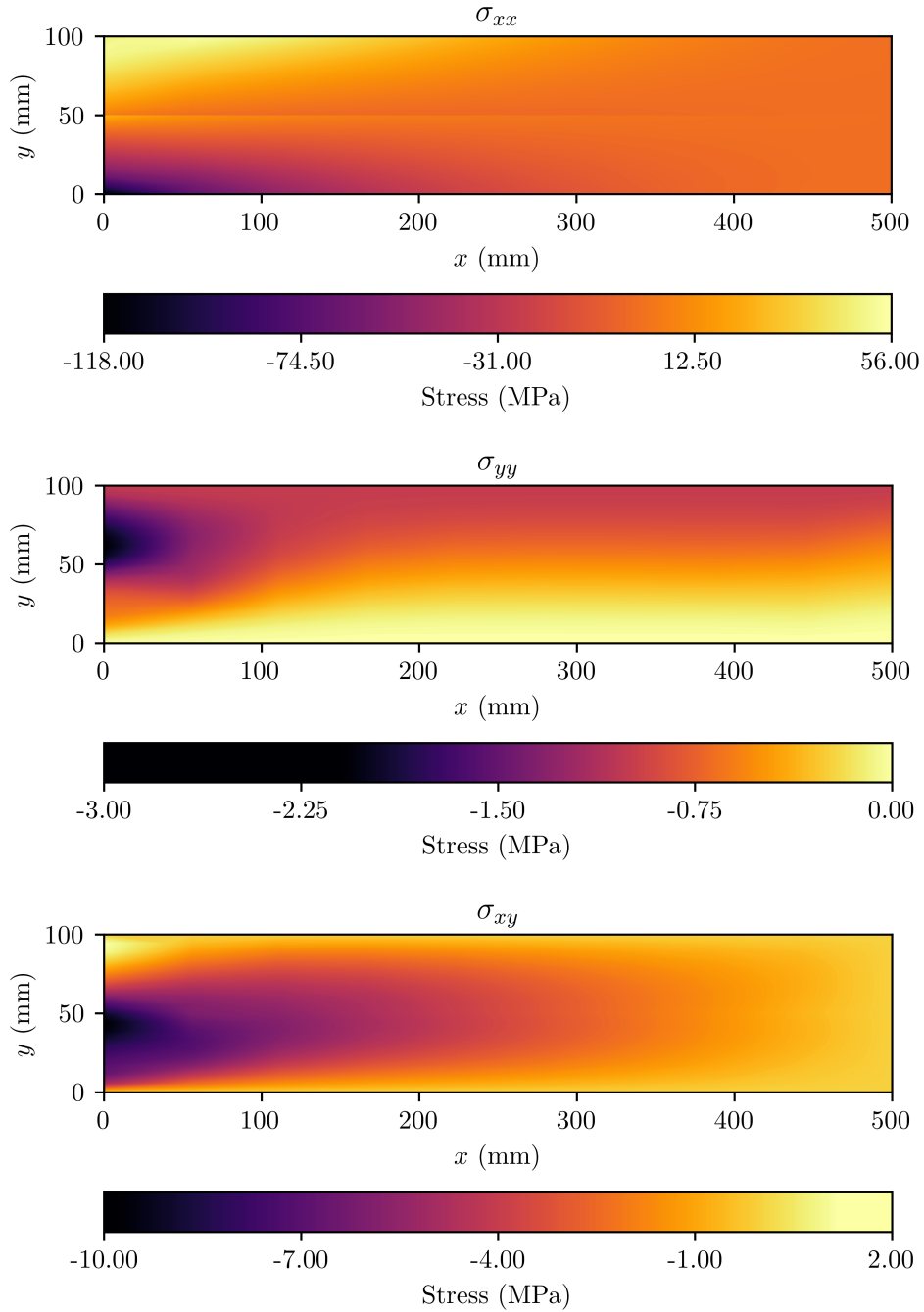


Figure 8: Bi-layer cantilever: stress distributions for the three stress components.

(element code CPS4). The elements were arranged in a structured mesh with a characteristic element size of $\delta^{\text{ref}} = 0.25$ mm, determined through a mesh convergence study. In contrast, our spline-based model employs $\mathcal{N} = 168$ unknowns and, using uniform open knot vectors, 30 elements per layer, resulting in 60 elements in total. This corresponds to an element area of

$$\Delta A = \frac{L \cdot (H_1 + H_2)}{60} \approx 833.33 \text{ mm}^2, \quad (33)$$

and a characteristic element length of $\delta = \sqrt{\Delta A} \approx 29$ mm. Compared to the element length used in the reference with $\delta^{\text{ref}} = 0.25$ mm, our characteristic element length is roughly two orders of magnitude larger. Since the number of elements in a structured mesh grows quadratically with the inverse of the element size, this corresponds to a difference of roughly four orders of magnitude in the number of unknowns. We will show that despite this drastic reduction, our spline-based approach still yields stress predictions in excellent agreement with the FEM solution.

The comparison focuses on the axial stress σ_{xx} and the shear stress σ_{xy} evaluated across the beam height at two positions along the beam: $x = 250$ mm and $x = 375$ mm. As shown in Figure 9, the axial stress exhibits a clear discontinuity at the material interface, which is also accurately captured by the spline-based approach. The shear stress, in contrast, shows an asymmetric yet continuous profile that again matches well with the FEM results. These results demonstrate that the spline-based formulation can deliver accurate stress predictions with a drastically reduced number of DOFs, highlighting its efficiency even in complex scenarios.

3.3. Parabolic-Shaped Cantilever

As a final test case, we consider a non-symmetric cantilever with a parabolic profile, leading to a non-prismatic cross section. This example serves to demonstrate the applicability of our approach to problems beyond geometrically regular, rectangular domains. The specific test case, assuming plane stress conditions, was originally introduced in [37, Section 4] and further examined in [38, Section 3.2] as a representative example of non-prismatic structural elements, which are commonly used in civil engineering applications.

The dimensions of the beam are illustrated in Figure 10. Over the beam length L , the height varies from H_0 at the fixed end to $H_L = H_0/2$ at the

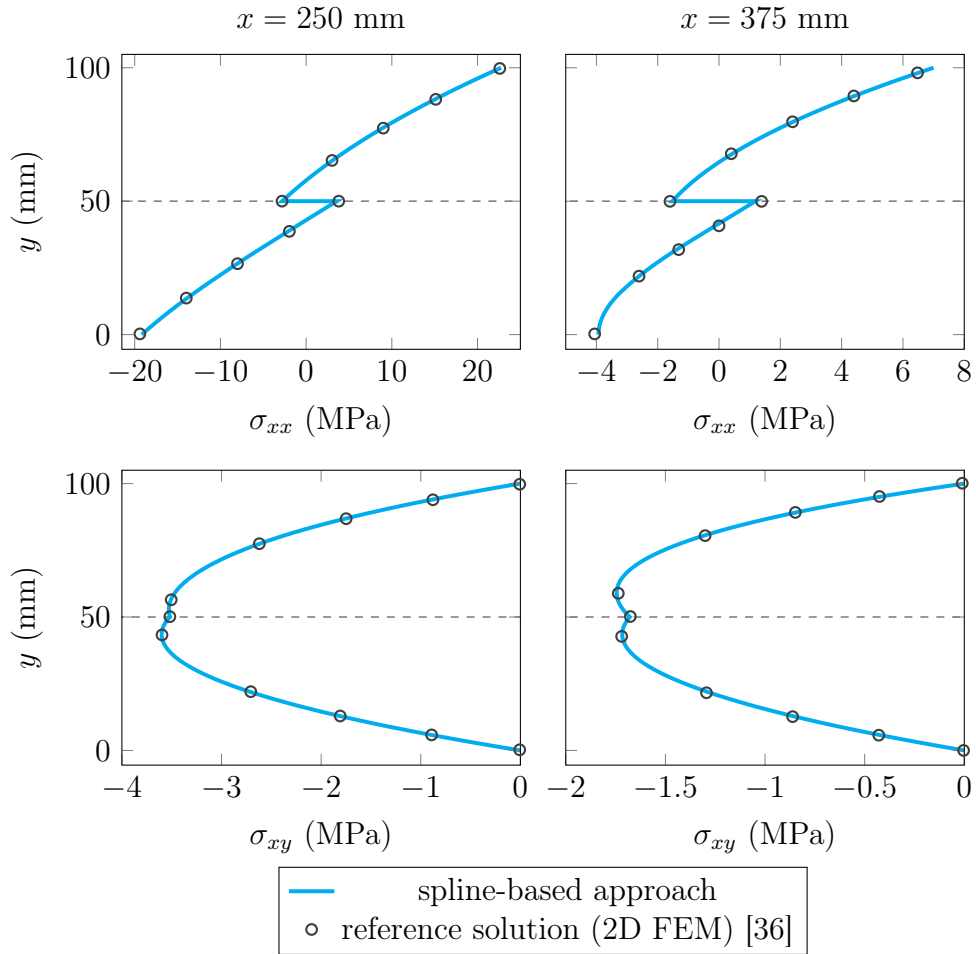


Figure 9: Bi-layer cantilever: comparison of the axial stress σ_{xx} (top row) and the shear stress σ_{xy} (bottom row) evaluated across the beam height at two positions: $x = 250$ mm (left column) and $x = 375$ mm (right column).

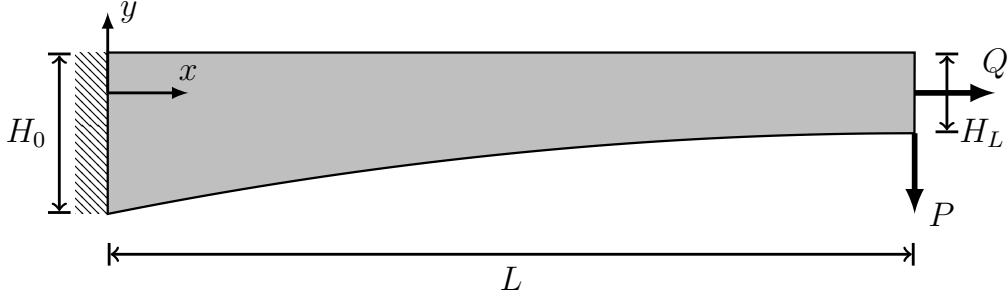


Figure 10: Parabolic-shaped cantilever: setup.

L (m)	H_0 (m)	H_L (m)	Q (kN)	P (kN)	E (Pa)	ν (-)
5	1	0.5	100	-100	1×10^5	0.3

Table 7: Parabolic-shaped cantilever: test case settings.

free end. While the upper edge remains horizontal, the lower edge follows a parabolic curve, resulting in an asymmetric, non-prismatic geometry. As before, it is assumed that the beam has a unit depth. At the right end, a horizontal force Q and a vertical force P are applied. The specific values for the geometric dimensions, loading conditions, and material parameters are listed in Table 7.

For the spline-based approach, the resulting geometric mapping is given by

$$\mathbf{T}(\xi, \eta) = \left(\begin{array}{c} \xi L \\ \frac{H_0}{4} (2\eta + (1 - \eta) (-2\xi^2 + 4\xi - 2) - 1) \end{array} \right). \quad (34)$$

We choose polynomial degrees $p = 6$ and $q = 4$, and define a control net consisting of $n = 10$ by $m = 5$ control variables, yielding a total of $\mathcal{N} = 50$. Along the top and bottom edges, zero-traction conditions are applied, while on the right edge the loading is enforced through traction conditions with equivalent resultant forces. As before, the zero-displacement condition on the left edge is implicitly enforced through the total complementary energy and requires no additional treatment. An overview of the weakly enforced boundary conditions is provided in Table 8.

Figure 11 presents the resulting stress distributions for the three stress components. Due to the non-prismatic geometry and the combined loading

	Horizontal	Vertical
Top	$\int_0^L t_i ^2 dx$	
Bottom	$\int_0^L t_i ^2 dx$	
Right	$\left(\int_0^{H_L} t_x dy - Q\right)^2$	$\left(\int_0^{H_L} t_y dy - P\right)^2$

Table 8: Parabolic-shaped cantilever: quantities to be minimized for a weak enforcement of the boundary conditions.

conditions, the stress fields exhibit complex, non-trivial patterns. Despite this complexity, the spline-based formulation yields smooth and coherent stress fields. As in the previous example, we assess their accuracy by comparison with a reference FEM solution reported in the literature [38, Section 3.2]. The reference solution was computed using Abaqus with a structured mesh of 2000×150 4-node bilinear plane stress elements (element type CPS4). Unlike the previous test case, where a characteristic element length was used for comparison, the geometry of the beam in this case prevents a straightforward definition of such a length. Since the reference does not specify one either, we instead estimate the resulting number of unknowns as $\mathcal{N}^{\text{ref}} \approx 6 \times 10^5$ DOFs. In contrast, the spline-based approach uses only $\mathcal{N} = 50$ unknowns, representing a reduction of four orders of magnitude. This aligns with the efficiency gains observed in the previous test case. As before, we now assess whether the spline-based formulation can still provide accurate stress predictions when compared to the detailed FEM reference solution.

Specifically, we compare the transverse normal stress σ_{yy} and the shear stress σ_{xy} at the mid-span of the beam ($x = 2.5$ m). Their distribution across the beam’s height is shown in Figure 12. The comparison demonstrates excellent agreement between the spline-based solution and the FEM reference, with the spline-based approach accurately capturing the overall stress profiles but also localized features like the inflection point in σ_{yy} . This highlights the effectiveness of the proposed approach also in geometrically more complex domains.

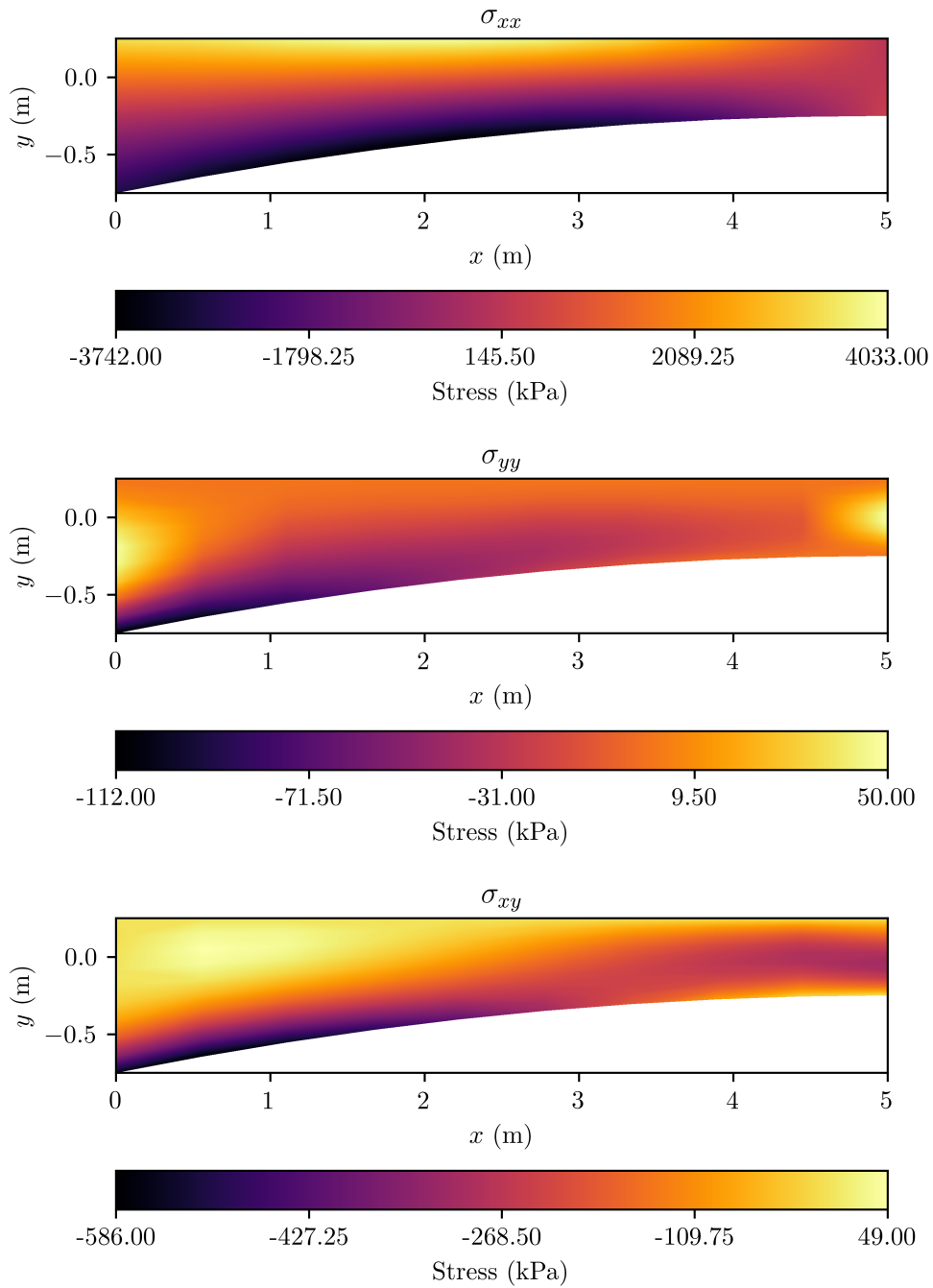


Figure 11: Parabolic-shaped cantilever: stress distributions for the three stress components.

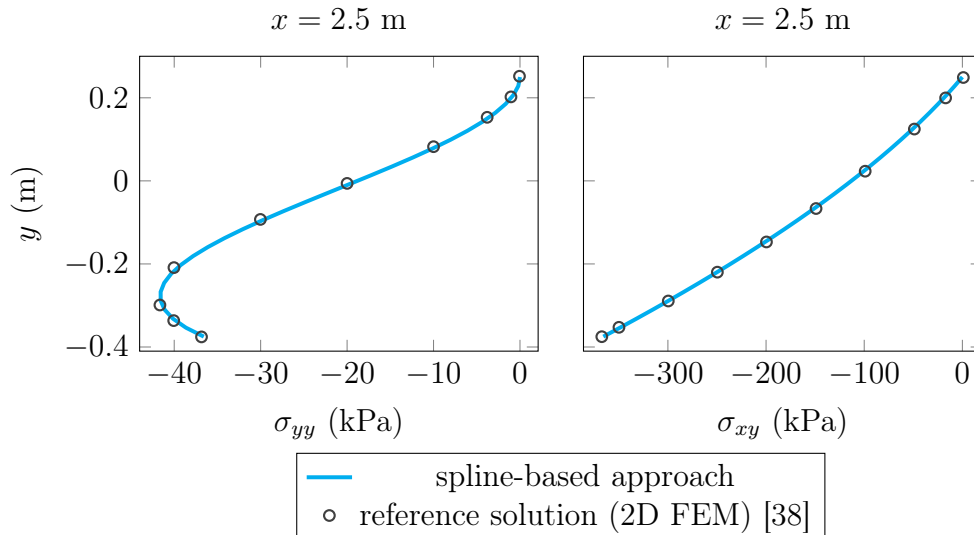


Figure 12: Parabolic-shaped cantilever: comparison of the transverse normal stress σ_{yy} (left) and the shear stress σ_{xy} (right) across the beam’s height at the mid-span ($x = 2.5 \text{ m}$).

4. Conclusion and Outlook

In this work, we presented a spline-based formulation for stress prediction in two-dimensional linear elasticity problems. The method is based on a B-spline discretization of the Airy stress function over a parametric domain. By introducing a geometric mapping, complex physical domains can be effectively represented. Thanks to the characteristics of the B-spline basis functions and their derivatives, the incorporation of traction boundary conditions and additional constraints is greatly simplified. The resulting stress fields are obtained through a variational approach, specifically the principle of minimum total complementary energy.

To assess the performance of the proposed approach, we conducted a series of numerical experiments, which demonstrated several key strengths of the method. First, validation against a power series solution confirmed the accuracy of the spline-based formulation for a classical benchmark problem including the bending of a beam by uniform transverse loading.

We then applied the method to more challenging scenarios involving either complex material behavior or non-trivial geometry. Specifically, we investigated (1) a bi-layer cantilever composed of anisotropic materials, and (2) a

cantilever with a non-prismatic, parabolic profile. In both cases, comparisons with high-resolution FEM reference solutions from the literature showed excellent agreement in the stress fields. Notably, the spline-based approach achieved the same level of accuracy with a number of unknowns that was four orders of magnitude smaller than that of the reference models.

Together, these results demonstrate that the proposed formulation effectively addresses the limitations of conventional methods: analytical approaches are often restricted to simple problems, while FEM approaches, either displacement- or stress-based, typically require a large number of unknowns to obtain accurate stress predictions.

Nonetheless, the approach also comes with certain limitations that define its current scope. These limitations are rooted both in the underlying methodology, i.e., the use of the Airy stress function and the principle of minimum complementary energy, as well as in the chosen approximation framework. First, the formulation is restricted to linear elasticity to ensure that we can apply the principle of minimum complementary energy. While extensions to geometrically nonlinear settings have been investigated, such generalizations remain an active area of research, as discussed in [39]. Second, the assumption of plane problems arises directly from the use of the Airy stress function. Finally, B-splines were used for the approximation due to the ease of implementation.

Despite these limitations, the presented formulation opens up promising directions for further research and application. Future work may focus on extending the method to three-dimensional problems through alternative stress functions, or on enhancing the expressiveness of the stress representation by employing more general spline-based bases such as NURBS. These developments could significantly broaden the scope and applicability of the proposed approach.

Beyond these potential extensions, the methodology is already relevant for ongoing developments in applied mechanics. For instance, a recent formulation of structural design optimization for quantum annealing (QA) [40] builds upon the principle of minimum complementary energy. Since QA requires unconstrained minimization problems, the presented stress function-based approach, which automatically satisfies the constraint of static admissibility, offers a substantial benefit. Similarly, in the context of data-driven material identification using physics-informed neural networks (PINNs) [41], the

use of a stress function ensures internal equilibrium by construction, making it an attractive option for embedding physical consistency into the learning process.

References

- [1] M. H. Sadd, *Elasticity: Theory, Applications, and Numerics*, 4th Edition, Academic Press, 2021. doi:10.1016/C2017-0-03720-5.
- [2] J. N. Reddy, *Energy principles and variational methods in applied mechanics*, 3rd Edition, John Wiley & Sons, Hoboken, USA, Chichester, UK, 2017.
- [3] G. B. Airy, On the strains in the interior of beams, *Philos Trans R Soc Lond* 153 (1863) 49–79. doi:10.1098/rstl.1863.0004.
- [4] C.-Y. Neou, A direct method for determining airy polynomial stress functions, *J Appl Mech* 24 (1957) 387–390. doi:10.1115/1.4011551.
- [5] B. F. de Veubeke, *Displacement and equilibrium models in the finite element method*, John Wiley & Sons, 1965.
- [6] O. C. Zienkiewicz, *Displacement and equilibrium models in the finite element method* by B. Fraeijs de Veubeke, Chapter 9, Pages 145–197 of *Stress Analysis*, Edited by O. C. Zienkiewicz and G. S. Holister, Published by John Wiley & Sons, 1965, *Int J Numer Methods Eng* 52 (2001) 287–342. doi:10.1002/nme.339.
- [7] H.-C. Hu, On some variational principles in the theory of elasticity and the theory of plasticity, *Sci Sin* 10 (1954) 259–290. doi:10.7498/aps.10.259.
- [8] K. Washizu, *On the variational principles of elasticity and plasticity*, Tech. rep. (1955).
- [9] E. Hellinger, Die allgemeinen Ansätze der Mechanik der Kontinua, in: F. Klein, C. Müller (Eds.), *Encyklopädie der mathematischen Wissenschaften mit Einschluss ihrer Anwendungen*, Vol. 4, B.G. Teubner, 1914, pp. 601–694.

- [10] E. Reissner, On a variational theorem in elasticity, *J Math Phys* 29 (1950) 90–95. doi:10.1002/sapm195029190.
- [11] E. Reissner, A note on variational principles in elasticity, *Int J Solids Struct* 1 (1965) 93–95. doi:10.1016/0020-7683(65)90018-1.
- [12] T. J. R. Hughes, *The Finite Element Method: Linear Static and Dynamic Finite Element Analysis*, Dover Publications, 2000.
- [13] T. J. R. Hughes, J. A. Cottrell, Y. Bazilevs, Isogeometric analysis: CAD, finite elements, NURBS, exact geometry and mesh refinement, *Comput Methods Appl Mech Eng* 194 (2005) 4135–4195. doi:10.1016/j.cma.2004.10.008.
- [14] J. A. Cottrell, T. J. Hughes, Y. Bazilevs, *Isogeometric Analysis: Toward Integration of CAD and FEA*, John Wiley & Sons, Ltd, 2009. doi:10.1002/9780470749081.
- [15] T. H. H. Pian, Derivation of element stiffness matrices by assumed stress distributions, *AIAA J* 2 (1964) 1333–1336. doi:10.2514/3.2546.
- [16] B. F. D. Veubeke, O. C. Zienkiewicz, Strain-energy bounds in finite-element analysis by slab analogy, *J Strain Anal* 2 (4) (1967) 265–271. doi:10.1243/03093247V024265.
- [17] E. F. Rybicki, L. A. Schmit, An incremental complementary energy method of nonlinear stress analysis, *AIAA J* 8 (1970) 1805–1812. doi:10.2514/3.5994.
- [18] R. Gallagher, A. Dhalla, Direct flexibility finite element elastoplastic analysis, in: *Proc. 1st Int. Conf. Struct. Mech. React. Technol., IAS-MiRT*, 1971.
- [19] R. H. Gallagher, Finite element structural analysis and complementary energy, *Finite Elem Anal Des* 13 (1993) 115–126. doi:10.1016/0168-874X(93)90051-Q.
- [20] G. F. Carey, A. Kabaila, M. Utku, On penalty methods for interelement constraints, *Comput Methods Appl Mech Eng* 30 (1982) 151–171. doi:10.1016/0045-7825(82)90002-0.

- [21] C. V. G. Vallabhan, M. Azene, A finite element model for plane elasticity problems using the complementary energy theorem, *Int J Numer Methods Eng* 18 (1982) 291–309. doi:10.1002/nme.1620180210.
- [22] N. Sarigul, R. H. Gallagher, Assumed stress function finite element method: Two-dimensional elasticity, *Int J Numer Methods Eng* 28 (1989) 1577–1598. doi:10.1002/nme.1620280709.
- [23] E. Bertóti, Complementary energy method for cylindrical shells using second order stress functions, *Comput Methods Appl Mech Eng* 108 (1993) 147–163. doi:10.1016/0045-7825(93)90158-T.
- [24] S. Cen, X.-R. Fu, M.-J. Zhou, 8- and 12-node plane hybrid stress-function elements immune to severely distorted mesh containing elements with concave shapes, *Comput Methods Appl Mech Eng* 200 (2011) 2321–2336. doi:10.1016/j.cma.2011.04.014.
- [25] A. Montanino, D. D. Gregorio, C. Olivieri, A. Iannuzzo, The continuous Airy-based for stress-singularities (CASS) method: an energy-based numerical formulation for unilateral materials, *Int J Solids Struct* 256 (2022) 111954. doi:10.1016/j.ijsolstr.2022.111954.
- [26] A. K. Pour, E. N. Farsangi, Airy stress function for proposed thermoelastic triangular elements, *J Eng Math* 138 (2023) 11. doi:10.1007/s10665-022-10256-1.
- [27] Z. Więckowski, P. Świątkiewicz, Stress-based FEM in the problem of bending of Euler–Bernoulli and Timoshenko beams resting on elastic foundation, *Materials* 14 (2021). doi:10.3390/ma14020460.
- [28] F. Fraternali, Complementary energy variational approach for plane elastic problems with singularities, *Theor Appl Fract Mech* 35 (2001) 129–135. doi:10.1016/S0167-8442(00)00054-9.
- [29] F. Fraternali, M. Angelillo, A. Fortunato, A lumped stress method for plane elastic problems and the discrete-continuum approximation, *Int J Solids Struct* 39 (2002) 6211–6240. doi:10.1016/S0020-7683(02)00472-9.
- [30] Y. Wang, J. Sun, T. Rabczuk, Y. Liu, Dcem: A deep complementary energy method for linear elasticity, *Int J Numer Methods Eng* 125 (2024) e7585. doi:10.1002/nme.7585.

- [31] A. Sky, A. Zilian, Symmetric unisolvent equations for linear elasticity purely in stresses, *Int J Solids Struct* 295 (2024) 112808. doi:10.1016/j.ijsolstr.2024.112808.
- [32] A. Sky, A. Zilian, Numerical analysis of the stress-based formulation of linear elasticity, *Proc Appl Math Mech* 24 (2024) e202400185. doi:10.1002/pamm.202400185.
- [33] F. Engesser, Über statisch unbestimmte Träger bei beliebigem Formänderungs-Gesetze und über den Satz von der kleinsten Ergänzungsarbeit, *Zeitschrift des Architekten-und Ingenieur-Vereins zu Hannover* 35 (1889) 733–744.
- [34] H. M. Westergaard, On the method of complementary energy, *Trans Am Soc Civ Eng* 107 (1942) 765–793. doi:10.1061/TACEAT.0005550.
- [35] N. J. Hoff, *The analysis of structures: based on the minimal principles and the principle of virtual displacements*, John Wiley & Sons, New York, NY, USA, 1956.
- [36] G. Balduzzi, S. Morganti, J. Füssl, M. Aminbaghai, A. Reali, F. Auricchio, Modeling the non-trivial behavior of anisotropic beams: A simple timoshenko beam with enhanced stress recovery and constitutive relations, *Compos Struct* 229 (2019) 111265. doi:10.1016/j.compstruct.2019.111265.
- [37] A. Beltempo, G. Balduzzi, G. Alfano, F. Auricchio, Analytical derivation of a general 2D non-prismatic beam model based on the Hellinger–Reissner principle, *Eng Struct* 101 (2015) 88–98. doi:10.1016/j.engstruct.2015.06.020.
- [38] V. Mercuri, G. Balduzzi, D. Asprone, F. Auricchio, Structural analysis of non-prismatic beams: Critical issues, accurate stress recovery, and analytical definition of the Finite Element (FE) stiffness matrix, *Eng Struct* 213 (2020) 110252. doi:10.1016/j.engstruct.2020.110252.
- [39] H. A. F. A. Santos, Complementary-energy methods for geometrically non-linear structural models: An overview and recent developments in the analysis of frames, *Arch Comput Methods Eng* 18 (2011) 405–440. doi:10.1007/s11831-011-9065-6.

- [40] F. Key, L. Freinberger, A formulation of structural design optimization problems for quantum annealing, *Mathematics* 12 (3) (2024). doi:10.3390/math12030482.
- [41] B. van der Heijden, X. Li, G. Lubineau, E. Florentin, Enforcing physics onto PINNs for more accurate inhomogeneous material identification, *Comput Methods Appl Mech Eng* 441 (2025) 117993. doi:10.1016/j.cma.2025.117993.